Optical and Quantum Electronics (2024) 56:636
https://doi.org/10.1007/s11082-024-06308-8

The investigation of structural, electronic, thermal, and elastic properties of X_2ZnH_4 (X = K, Rb and Cs) for hydrogen storage applications: DFT study

Hafeez Ur Rehman[1] · Nawaz Muhammad[1] · G. Murtaza[1] · Hafiz Hamid Raza[1] · Shahid M. Ramay[2] · M. Irfan[3] · M. Awais Rehman[4]

Received: 3 July 2023 / Accepted: 5 January 2024 / Published online: 5 February 2024

Abstract
Hydrogen storage in the solid state method focuses more on attraction and requires large-scale research. Ab initio calculations of zinc-based Alkali metal hydrides X_2ZnH_4 (X = K, Rb and Cs) were performed to analyse the structural, electronic, thermal, and elastic properties. Studied hydrides are stable in the orthorhombic phase with space group16- PP222. Phonon dispersion curves are calculated at ambient conditions reveals thermodynamic stability. Electronic band structures and density of states reveal that these hydrides are direct bandgap semiconductors. Also, thermoelectric properties like thermal conductivity, electrical conductivity, specific heat capacity, Seebeck coefficient, Hall coefficient and carrier concentration are investigated using BoltzTraP software. In addition, the elastic constants have been calculated, and the mechanical properties such as bulk modulus, shear modulus, Young's modulus and Poisson's ratio have been calculated using these elastic constants. According to well-known Born stability criteria, K_2ZnH_4 and Rb_2ZnH_4 are mechanically stable, while Cs_2ZnH_4 is unstable. These hydrides might be used in hydrogen storage applications due to moderate gravimetric hydrogen density, which is 2.7 wt%, 1.6 wt%, 1.2 wt% for K_2ZnH_4, Rb_2ZnH_4, Cs_2ZnH_4, respectively.

Keywords Density functional theory · Hydrogen storage · Ab initio calculations · Thermoelectric properties

1 Introduction

Today's overpopulated areas face poor air calibre and a fast-decreasing rate of energy origins worldwide. This quick utilisation rate has materialised the need for cleaned, improved, and feasible energy derivations. In many natural resources, hydrogen has tremendous focus as a coherent energy transporter, and it can be free from carbon if it is produced from sustainable sources. If it is made, there are many ways to store hydrogen in gas, liquid, or solid-state form. However, every choice has supremacy; not everyone assures the critical specifications such as price, security, pressure, and energy compactness for practical applications. Adsorption of hydrogen on the surface of solid- or solid-state hydrogen storage

Extended author information available on the last page of the article

is preferable to achieve a secure, structured, and excessive amount of hydrogen storage, particularly for transportation. For practical implementation of hydrogen storage, solids require materials with less weight, elevated hydrogen compactness, and suitable adsorption and desorption temperature (Zhang et al. 2016). Metal hydrides are preferred for hydrogen storage with hydrogen storage by weight from 5–8 wt. % (Niaz et al. 2015). Like MgH_2 and LiH, these hydrides still tolerate High thermal solidity and low reaction kinetics (Wang et al. 2018; Qi et al. 2023). The characteristics of Mg–Al alloys were experimentally studied by Anderson. In addition and removal of the hydrogen process of MgH_2, it seemed that the insertion of Al boosts the system's kinetics. Compounds like $LiBH_3$ and $NaBH_3$, Mg $(BH_2)_2$ and Ca $(BH_2)_2$ with greater hydrogen concentration are yet under consideration to remove the formation of Borane during the reaction (Chen 2023). Elastic effects of $NaMgH_3$ were studied using Ab initio calculations (Reshak et al. 2011). $LiBeH_3$ and $NaBH_3$ show mechanical and thermal stabilities. But Be is not preferred because of its magnetic properties (Chen and Yu 2023; Wang et al. 2023). Perovskite-type hydrides like $KMgH_3$, $SrLiH_3$, and $BLiH_3$ are pondered due to their lightweight, stable conditions and site of hydrogen (Zaluska et al. 2000). Thermal, electronic, and optical properties of $LiBaH_3$, $LiSrH_3$, and $LiCsH_3$ are studied, and it found that $LiBaH_3$ is more stable than $LiSrH_3$; conversely, $LiCsH_3$ is considered to be unstable (Bertheville et al. 2001). Due to their potential as a material for handling hydrogen and tritium as storage, availability, and rehabilitation in thermonuclear fusion devices, the AB-type zirconium-based alloy family, which includes ZrNi and ZrCo, has gained a lot of interest to date (Wang et al. 2021, 2022). This is because the stimulation process is easy, its absorption characteristics are excellent, and the kinetics of the hydrogen breakdown are high. Furthermore, they exhibit an adequate equilibrium pressure of tritium at ambient and mild temperatures for releasing tritium gas at atmospheric pressure (Zhao et al. 2023; Lu et al. 2017). The recent focus on ternary metal hydrides has been seen as a new direction for pressure-dependent high-temperature superconductor research. This is largely due to the wide variety of ways that metals even metalloids can be alloyed with hydrogen. New stages of $Mg-B-H$ ternary hydrides can be anticipated here using first-principles evolutionary techniques. As a consequence, associated phonon and electrical calculations for the three a candidate phases are carried out one after the other to verify their potential to become conductors and their dynamic stability. The recent focus on ternary metal hydrides has been seen as a new direction for pressure-dependent high-temperature superconductor research. This is largely due to the wide variety of ways that metals even metalloids can be alloyed with hydrogen. New stages of $Mg-B-H$ ternary hydrides can be anticipated here using first-principles evolutionary techniques. As a consequence, associated phonon and electrical calculations for the three a candidate phases are carried out one after the other to verify their potential to become conductors and their dynamic stability (Sukmas et al. 2023; Pluengphon et al. 2022). Magnesium-based ternary alkaline-earth hydrides are important to create new transition metal hydrides. In contrast to the strontium and barium-containing systems, which contain accordingly three (Sr_2MgH_6, $SrMgH_4$, $Sr_2Mg_3H_{10}$ and four (Ba_2MgH_6, $BaMgH_4$, $Ba_5Mg_7H_{26}$, $Ba_2Mg_3H_{10}$ ternary hydride phases, only one such step is known for the calcium-containing system ($Ca_4Mg_3H_{14}$.report on the synthesis and crystal structure of a second ternary hydride phase of composition $Ca_{19}Mg_8H_{54}$. High-pressure synthesis was used to create the chemical, and it was discovered to be isostructural with Yb_{19} Mg_8H_{54} (Pluengphon et al. 2021).

One of the building block groups for the solid-state storage of hydrogen is perovskite-type hydrides. Perovskite-type hydrides with the ABH_3 formula demonstrate high gravimetric storage of hydrogen features. Since perovskite-type hydrides typically consist of

1A to 2A group elements, there aren't many. $NaMgH_3$ has been the subject of the most research. $LiNiH_3$ perovskite type hydride has been created and studied in the literature utilising theoretical modelling and in situ synchrotron X-ray diffraction. $LiNiH_3$ research is intriguing since it contains nickel, an element from the 8B group (Lu et al. 2023; Huang 2023). There are a couple of perovskite hydrides (X = H) situations in addition to chalcogenides and chalcogenides. The ternary metal hydrides indicate a saline coupling property when A and B are monovalent alkali (M) and divalent alkaline earth metals (Ae). For preserving hydrogen at extreme temperatures, certain hydrides are of interest. The perfect perovskite structure has been found in five reported hydrides: $CsCaH_3$, $RbCaH_3$, $KMgH_3$, $BaLiH_3$, and $SrLiH_3$. Due to the singly charged M cation filling the octahedral gaps, the latter is sometimes called inverse perovskites. $LiBeH_3$, a light metal hydride, has also been hypothesized to adopt the cubic perovskite structure and exhibit high-temperature superconductivity. However, $LiBeH_3$'s composition and characteristics have been scrutinized (Feng et al. 2023; Qiu et al. 2023a).

Lithium-based compounds such as Li_2BeH_4 and, K_2MgH_4 (Adimi et al. 2017), Li_2MgH_4 are investigated experimentally, and Mechanical, vibrational hydrogen storage properties regarding phase transitions are studied by using DFT calculations (Sun et al. 2023). Hydrides of aluminium contemplate as a good candidate for solid-state materials. Adami et al. investigated the phase shift of $AALH_4$(A = Li, Na, K, Rb, Cs) (Yao et al. 2020). Many magnesium-related compounds, such as Mg_2FeH_6, Mg_2NiH_4, and Mg_2CoH_5 were offered for hydrogen storage (Wimmer 2005; Broom 2011a). However, no one still meets the requirements for practical usage. Regarding storing high-density hydrogen storage, competence with natural resources fuels (Qiu et al. 2023b), economically suitable, increased productivity and secure practical applications, it is required to search for new materials. To achieve that, it needs to search for materials with good combinations and crystalline shapes. From this point of view, computational technique in the science of materials provides three leading facilities to explore the globe: superior knowledge of substances at the atomic level (Sheng et al. 2023), speculation of the consequences and clarifying the physical and chemical effects of substances proceeding to observations (Zhao et al. 2020; Yang et al. 2022). For some years, with the help of computers, efficiency and approach to more complex systems and calculations give rise to characteristics of materials in a considerable explanation. Enormous details about the material properties can be found using DFT calculations. Thermodynamic properties can be calculated by finding the energy difference between an ideal crystal and a deformed crystal. Likewise, vibrational and phonon trends of materials can be found by calculating the force on the remaining atoms and by detaching the pressure on these atoms (Jia et al. 2023; Kuang et al. 2018). DFT calculations can also be used to find out the elastic properties by reactions of materials concerning distortion. Using this method new hydrogen storage materials can be evaluated with accurate connections ahead with systematic, elastic, electrical, and optical characteristics without the requirements of costly experimental chains. M.Bortz et al. Studied the Rb_2ZnH_4 and Cs_2ZnH_4 by preparing the stoichiometric quantity of the above hydrides and with Zinc powder with the pressure of 80 bar at 650 K. Experimental investigations of the alkali hydrides show that the studied compounds are isotopic with K_2ZnH_4. This study's first time theoretical approach has been to study the Rb_2ZnH_4, Cs_2ZnH_4 and K_2ZnH_4 using density functional theory calculations. Substituting Zn is expected to enhance the hydrogen sorption properties and produce changes in formation enthalpy. This way is also preferable to reserve resources, time, and workforce. Due to this reason, in this study, we reasonably and comprehensively construct metal hydrides for hydrogen storage, by using density functional theory calculations. Firstly, we propose and predict the crystalline shape of K_2ZnH_4, Rb_2ZnH_4, and Cs_2ZnH_4 metal hydrides, recognize their structural and electronic properties. In the end,

absorption of these hydrides is calculated and examined. Since these calculations only need atomic numbers and crystal shapes as inputs. We initially studied their Gravimetric Hydrogen Density. That framework is the starting clue to this action. The gravimetric hydrogen density is an essential factor in this process, so the GHD of the studied compounds is calculated by using the following equation (Broom 2011b).

$$C_{wt\%} = \left(\frac{\left(\frac{H}{M}\right) M_H}{M_{Host} + (H/M) M_H} \times 100 \right) \% \tag{1}$$

where H/M denotes the ratio of hydrogen to metal, M_H represents the molar mass of hydrogen and M_{Host} is the molar mass of host material. The gravimetric hydrogen density for the studied compounds is 2.7 wt.%, 1.6 wt.% and 1.2 wt.% for K_2ZnH_4, Rb_2ZnH_4, and Cs_2ZnH_4 respectively.

2 Computational details

Ab initio calculations have been used to perform the structural, electronic, thermal, and elastic properties of zinc base hydrides by using the full-potential linearized augmented plane wave method within the framework of DFT by using WIEN2k Code. The generalized gradient approximation (GGA-PBE) proposed by Perdew-Burke-Ernzerhof parameterizes the exchange–correlation energy. The self-consistent calculations stop when the energy convergence reaches 0.001 Ry. In this method, the generalized gradient approximation (GGA) was used for the exchange–correlation potential to calculate structural and electronic properties (Rehmat et al. 2017). Perdew-Burke-Ernzerhof sol approximation was used to optimise the orthorhombic structure of X_2ZnH_4(X = K, Rb, Cs) by applying Birch Murnaghan's equation of state. The calculations are performed using RMT*K_{max} = 10 which is used to achieve the convergence in the first Brillion Zone. Here, R_{MT} and K_{max} muffin tin sphere and the largest K vector in-plane wave, respectively (Reshak and Jamal 2012). The cutoff energy for the separation between core and valence energy states was set equal to a value of −9.0 Ry (Santhosh et al. 2015). A denser mesh of k-points was used for the calculation of bandgap. Energy strain methods were performed to calculate elastic constants within the framework of the WIEN2k package (Murtaza et al. 2021). IRelast package implemented in WIEN2k code is used to calculate elastic constants. Elastic constants such as bulk modulus (B), shear modulus (G), Young's modulus (E) and Pugh's ratio (B/G) were.

calculated based on Voigt-Reuss-Hill approximation. Thermoelectric properties of the materials are computed by the semiclassical Boltzmann hypothesis, which is implemented in BoltzTrap. The transport properties are calculated by maintaining the constant relaxation time (Madsen and Singh 2006; Bulusu et al. 2008).

3 Results and discussion

3.1 Structural properties

As a first stage, the internal structure characteristics tune the X_2ZnH_4 (X = K, Rb and Cs) atom configuration. An initial investigation of the structure's qualities was conducted using

the obtained results. The equilibrium lattice constants and their first pressure derivative (B′) were determined by calculating the total energy at different volumes and fitting the result to the empirical Murnaghan's equation of state. Figure 2 depicts the change in total energy as a function of volume. Optimized structural parameters and the materials space group were also used to determine the atomic distances between the crystal's constituents. X_2ZnH_4 (X = K, Rb and Cs) has a centered orthorhombic structure and contains space group 16- PP222. The structural properties of X_2ZnH_4 (X = K, Rb and Cs) of the materials demonstrate orthorhombic structures with atomic positions are shown in Table 1 (Fig. 1).

The system's total energy is reduced to obtain the minimum point in the energy volume curve. For the implementation of this energy, two phases are important for this process. In the first one, the forces acting on one another inside the unit cell are executed. To get the energy versus volume curve, the total state of the system is calculated for a combination of the volume of the unit cell and c/a values in the second phase. The importance of X_2ZnH_4 has been streamlined by using the Birch-Murnaghan equation of state, and Hamiltonian variables have been calculated. Figure 2 demonstrates the total energy versus volume curves calculated at fixed equilibrium values of you and c/a ratio for K_2ZnH_4, Rb_2ZnH_4 and Cs_2ZnH_4. The underestimation of the lattice constants reveals that the GGA overestimates the volume. The calculated lattice constants, bulk modulus and its pressure derivative are summarised in Table 2.

In this study, the dynamical stability of the K_2ZnH_4, Rb_2ZnH_4, and Cs_2ZnH_4 hydrides is systematically investigated through the analysis of phonon dispersion curves (PDCs) obtained using the CASTEP software with the generalized gradient approximation (GGA). The supercells generated by PHONON software enable the construction of PDCs through the direct method, providing insights into the vibrational characteristics of the materials. The unit cells of these compounds contain 35 phonon branches, comprising 3 acoustic and 32 optic modes. Unlike the the absence of imaginary frequencies in the PDCs for K_2ZnH_4, Rb_2ZnH_4, and Cs_2ZnH_4 indicates their dynamical stability. The calculated phonon frequencies for K_2ZnH_4, Rb_2ZnH_4, and Cs_2ZnH_4 fall within the ranges of 4.4 THz, 4.5 THz, and 6 THz, respectively. There are no distinct bands attributed to large mass differences between constituent atoms, specifically H, K/Rb/Cs, and Zn. Interestingly, the absence of a gap between optical and acoustical modes further supports the dynamical stability of the compounds (Huang et al. 2022). At low frequencies, below 10 THz, the analysis of the PDCs reveals the predominant contributions to the acoustic and low-frequency optic phonon branches (Huang 2023). In summary, the presented phonon dispersion analysis demonstrates the dynamical stability of K_2ZnH_4,

Table 1 Used atomic positions and RMT

Compounds	Individual atoms	Atomic positions	Used RMT	Space group
K_2ZnH_4	K	0.5,0,0.5,0,0.5,0.5	1.3	**16-**PP222
	Zn	0,0,0	1.5	
	H	0.7,0.7,0.2,0.2,0.2,0.2,0.7,0.2, 0.7,0.2,0.7,0.7	0.9	
Rb_2ZnH_4	Rb	0.5,0,0.5,0,0.5,0.5	1.8	
	Zn	0.5,0,0.5,0,0.5,0.5	1.5	
Cs_2ZnH_4	Cs	0.5,0,0.5,0,0.5,0	2.2	
	Zn	0,0,0	1.5	

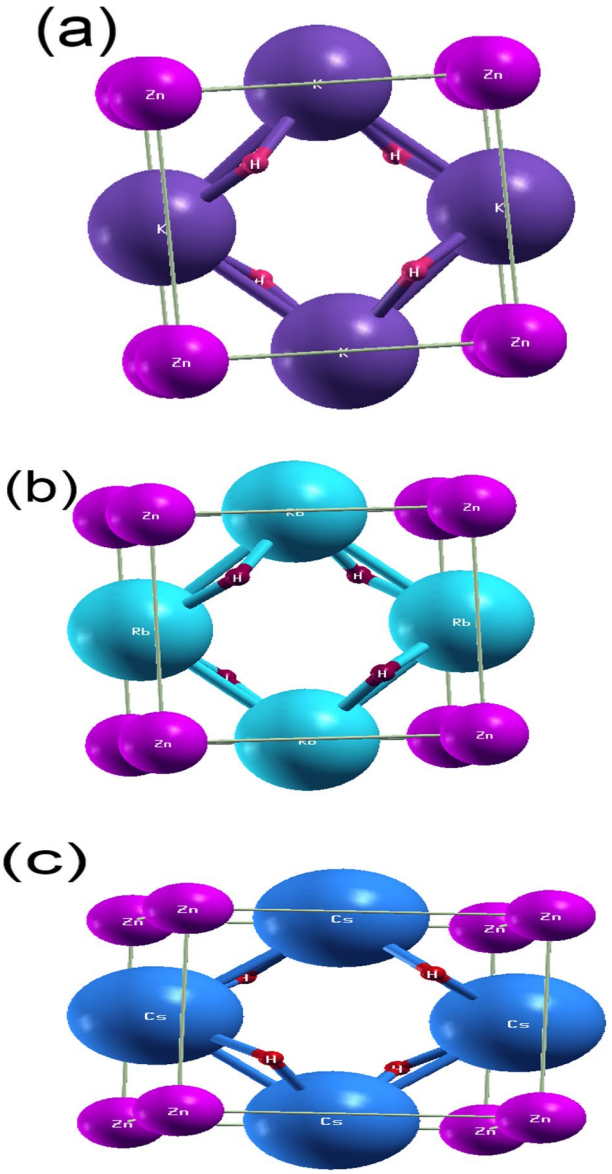

Fig. 1 Crystal structures of (**a**) K_2ZnH_4 (**b**) Rb2ZnH_4 (**c**) Cs2ZnH_4

Rb_2ZnH_4, and Cs_2ZnH_4 hydrides, providing valuable insights into their vibrational characteristics. The absence of imaginary frequencies, the frequency ranges obtained, and the contributions of individual atoms contribute to a comprehensive understanding of the materials' phonon behavior (Kuang et al. 2018), establishing a foundation. The phonon dispersion curves of X_2ZnH_4(X = K,Rb and Cs) are shown in Fig. 3. As there are no imaginary frequencies in the phonon spectra, therefore, all the studied materials are thermodynamically stable.

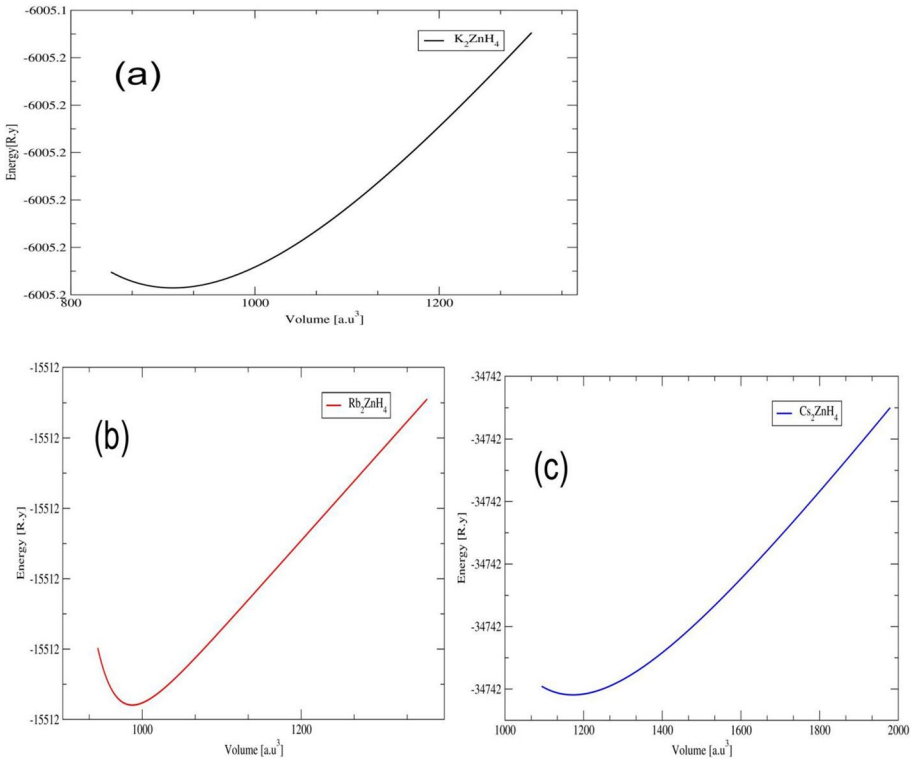

Fig. 2 Optimized curves of energy versus volume of (**a**) K_2ZnH_4 (**b**) Rb2ZnH$_4$ (**c**) Cs2ZnH$_4$

Table 2 The calculated lattice constants, the first derivative of bulk modulus (B') of K_2ZnH_4, Rb_2ZnH_4 and Cs_2ZnH_4

Compounds	Method	Approximation	Calculated cell parameters			B'	Experimental		
K_2ZnH_4	FP-LAPW	GGA	a	b	c		a	b	c
			10.5	10.9	11.0	16.28	7.7	5.8	10.2 (Bortz et al. 1994)
Rb_2ZnH_4	FP-LAPW	GGA	9.8	9.9	10.0	13.35	8.1	6.0	10.6 (Bortz et al. 1997)
Cs_2ZnH_4	FP-LAPW	GGA	9.8	9.2	10.0	3.98	8.5	6.3	11.1 (Bortz et al. 1997)

3.2 Electronic properties

The electronic properties of the materials are investigated by band structures along with the total and partial density of states. The electronic band structures of the zinc base alkali metal hydrides are shown in Fig. 4 (Robidas and Arivuoli 2014). Horizontal dotted lines represent the Fermi level. The bands appearing nearer to the Fermi level around -1 eV are due to the contribution of the H–s state electron. Hence, these hydrides can quickly free the hydrogen without extreme heating (Hussain et al. 2020). The energy band gap values for Zinc alkali hydrides X_2ZnH_4 (X = K, Rb, Cs) are 1.03 eV, 0.77 eV, and 0.26 eV,

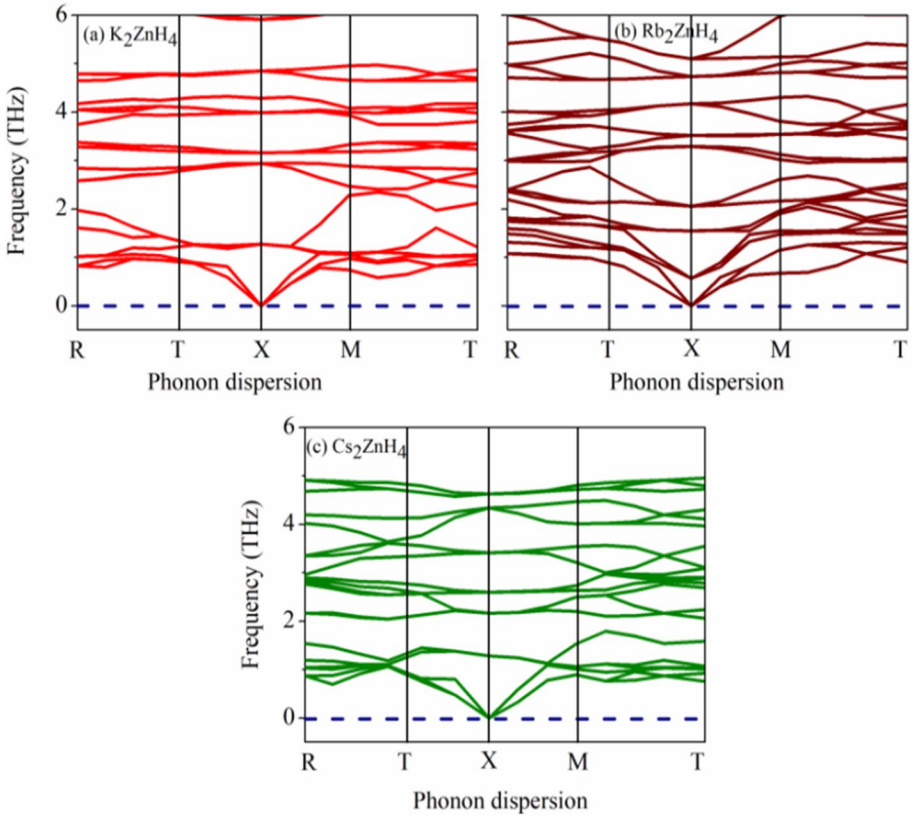

Fig. 3 Phonon dispersion curves of (**a**) K_2ZnH_4, (**b**) Rb_2ZnH_4 and (**c**) Cs_2ZnH_4

respectively. Thus, these hydrides are electronically semiconducting. From the bandgaps structure, valence band maxima and conduction band minima lie at the same symmetry point (Γ). Fundamental energy gaps represent the direct bandgap p-type nature of the materials (Subhan et al. 2019). In p-type semiconductors, the probability of finding a hole in the valence band is more significant than in the conduction band, so it means the occurring probability of electron will be more significant in the valence band, and as a result, the fermi level shifts towards the valence band (Li et al. 2019).

3.3 Density of states

To visualise the electronic dawns of band structures and to understand the electronic properties of the studied compounds, the total and partial density of states of the compounds X_2ZnH_4 (X = K, Rb, Cs) are estimated in the range of −4 to 6.5 eV by using the generalized gradient approximations. The total and partial density of states of X_2ZnH_4 (X = K, Rb, Cs) plots represent the valence and conduction bands around the Fermi level set at 0 eV, as shown in Fig. 5. The total and partial density of states reveals that in all materials X_2ZnH_4 (X = K, Rb, Cs), no conditions are present at the corner of the valence band and the Fermi level. However, the conduction bands are lying at relatively higher energy states. Hence, a significant energy gap is

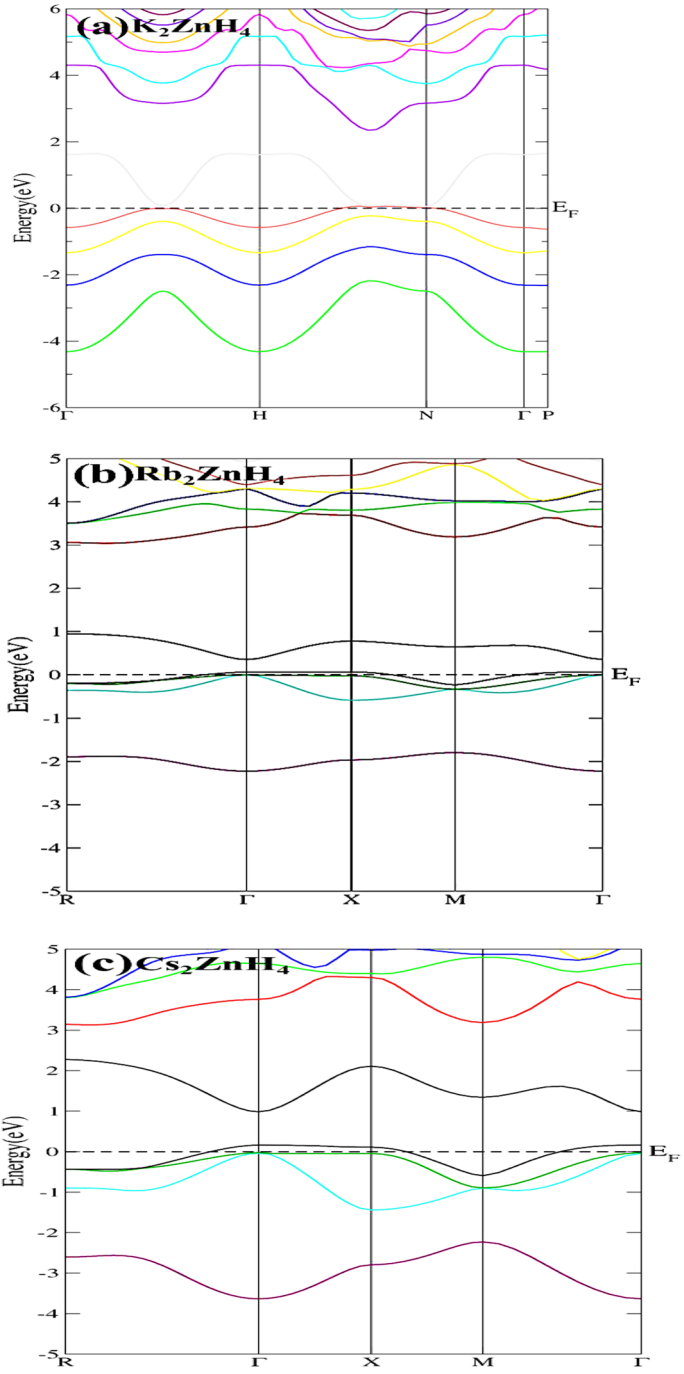

Fig. 4 The electronic band structures of (**a**) K_2ZnH_4 (**b**) Rb_2ZnH_4 and (**c**) Cs_2ZnH_4 compounds

present between the top of the valence band and the bottom of the conduction band. Therefore, it can be observed that these materials belong to semiconductors (Ali et al. 2018). From the plots of DOS, in K_2ZnH_4 peaks are observed near the top of valence and bottom of conduction bands due to the significant contribution of the d-state of zinc with the assistance of s and p-states of K along with the Hs-state while in Rb_2ZnH_4 p-state of Rb and Zn and s- state of hydrogen has significant contribution along with the minor contribution of s and d-state of Rb in the valence band and d-state of Rb has a significant contribution in the valence band. In the density of states of Cs_2ZnH_4, the d-state of Cs and p-state of Zn have the main role valence band.

3.4 Elastic properties

Elastic constants of the materials are used to investigate the mechanical stability of the materials. Elastic constants demonstrate the ratio of stress to strain, deforms in crystals, and the ability of materials to regain their original shapes and give information about forces and bonding charters (Li et al. 2019). Nine independent elastic constants are defined for an orthorhombic structure as C_{11}, C_{22}, C_{33}, C_{44}, C_{55}, C_{66}, C_{12}, C_{13}, and C_{23} (Al et al. 2020a). The well-known born stability criteria for orthorhombic structure are given as (Pugh et al. 1954).

$$
\begin{aligned}
&C_{11} + C_{33} - 2C_{13} > 0\, C_{22} + C_{33} - 2C_{23} > 0,\\
&C_{11} + C_{22} - 2C_{12} > 0,\ C_{11} > 0,\ C_{22} > 0,\\
&C_{33} > 0,\ C_{44} > 0,\ C_{55} > 0,\ C_{66} > 0,\\
&C_{11} + C_{22} + C_{33} + 2\left(C_{12} + C_{13} + C_{23}\right) > 0,\\
&1/3\left(C_{12} + C_{13} + C_{23}\right) < B < \left(C_{11} + C_{22} + C_{33}\right)
\end{aligned}
$$

The shear modulus(G) and bulk modulus(B) of the materials are calculated by elastic constants given in Eqs. 2 and 3 by

$$
\boldsymbol{G_V} = \frac{1}{15}\left[C_{11} + C_{22} + C_{33} - \left(C_{12} + C_{13} + C_{23}\right)\right] + \frac{3}{15}\left(C_{44} + C_{55} + C_{66}\right) \tag{2}
$$

$$
\boldsymbol{B_V} = \frac{1}{9}\left(C_{11} + C_{22} + C_{33} + 2C_{12} + 2C_{13} + 2C_{23}\right) \tag{3}
$$

The Hill average of Voigt and Reuss approximations gives the best indication of Bulk and shear modulus as follows.

$$
\boldsymbol{B} = \frac{\boldsymbol{B_V} + \boldsymbol{B_R}}{2} \tag{4}
$$

$$
\boldsymbol{G} = \frac{\boldsymbol{G_V} + \boldsymbol{G_R}}{2} \tag{5}
$$

Young's modulus (E) Pugh's criteria (B/G), and poissons's coefficient (υ) of the materials were calculated by following equations

$$
E = \frac{9BG}{3B + G} \tag{6}
$$

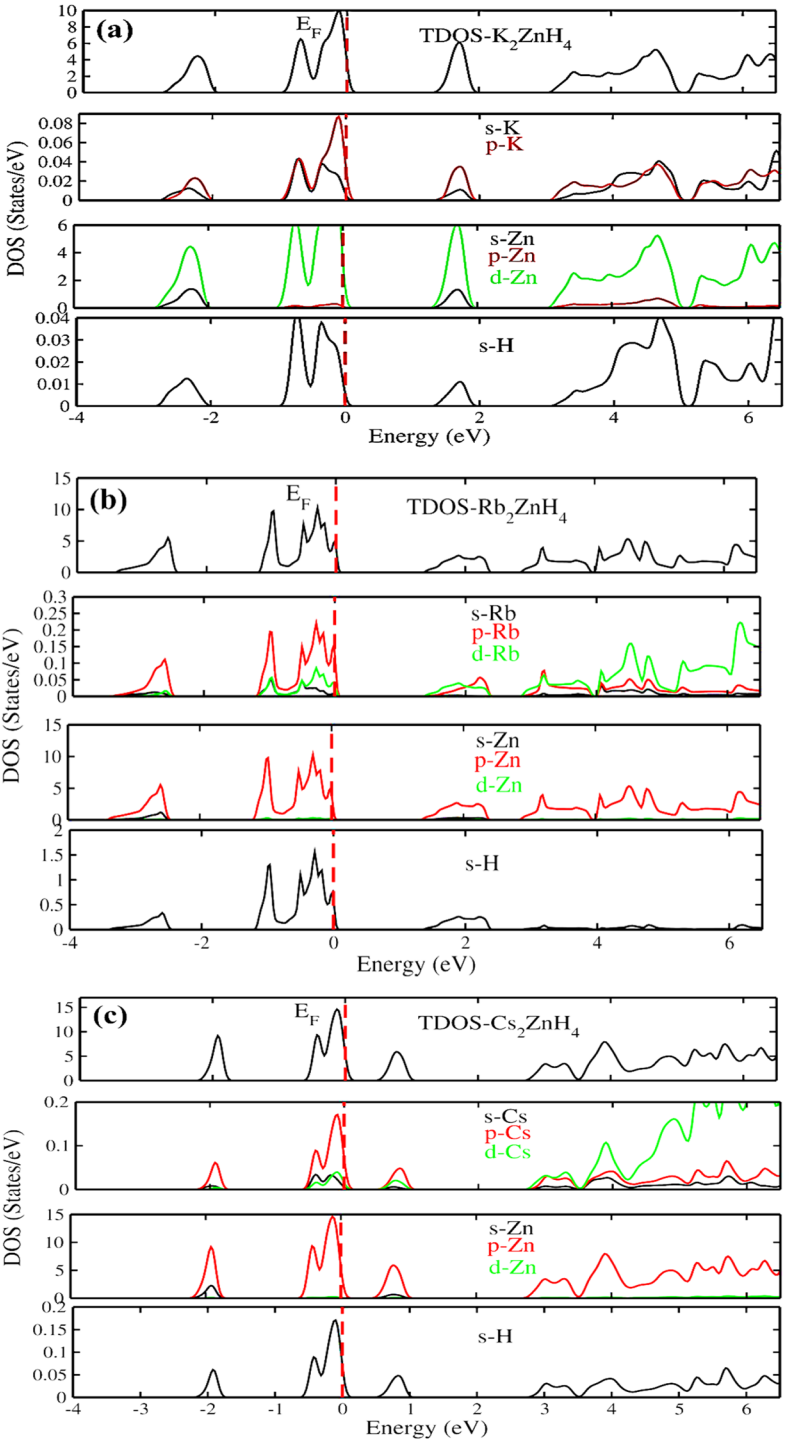

Fig. 5 Total and partial density of states of (**a**) K_2ZnH_4 (**b**) Rb_2ZnH_4 and (**c**) Cs_2ZnH_4 compunds

$$B/G = \frac{3B_H - 2G_H}{2(3B_H + G_{H)}} \tag{7}$$

$$\upsilon = \frac{3B - Y}{6B} \tag{8}$$

The estimated values of elastic constants are given in Table 2. The deals from Table 1 represent that the materials K_2ZnH4 Rb_2ZnH_4 are following the Born stability criteria, which indicate that both the materials are mechanically stable while the hydride Cs_2ZnH_4 is mechanically unstable. To find out the many unknown properties, critical parameters derived from elastic constants are given in Table 2. The bulk modulus of materials represents the resistance of materials towards volume change under the action of external stresses. Higher bulk modulus demonstrates the high resistance of materials against their volume change towards external pressures (Al et al. 2020b). It can be seen from Table 3 that Rb_2ZnH_4 has a higher value of bulk modulus than K_2ZnH_4, demonstrating that Rb_2ZnH_4 shows higher mechanical stability than K_2ZnH_4 while negative elastic constants of Cs_2ZnH_4can be found in low symmetry points (Pluengphon et al. 2021), and mechanically unstable than other two. Moreover, the Shear modulus of materials demonstrates the resistance of a material against shape change with the response of shear stresses. The shear modulus describes the hardness of materials better than the bulk modulus. The calculated shear modulus of Rb_2ZnH_4 is higher than K_2ZnH_4, and Cs_2ZnH_4 which is also in comparison with the results of the bulk modulus of compounds.

Pugh's criteria define the ductility and brittleness of materials by B/G ratio (Pugh et al. 1954); if a material has a lower percentage of B/G than 1.75 it explains that the material is brittle, and a higher value of B/G than 1.75 shows the flexibility of materials. According to the calculated results in Table 4 $K2ZnH_4$, Rb_2ZnH_4 and Cs_2ZnH_4 have B/G ratios of 1.05, 0.52 and 3.70, respectively. K_2ZnH_4 Rb_2ZnH_4 compounds have a lower B/G ratio than 1.75. Thus these compounds have a brittle nature. The brittle nature of the studied compounds is in comparison with Li_2CaH_4 and Li_2SrH_4. The brittle nature of the materials is due to the low B/G ratio of these alkali metal hydrides. This is an important parameter for materials, especially for transportation applications. The bonding nature of the material is defined by Poisson's ratio, which is perpendicular contraction and expansion when stresses are applied. The material shows covalent bonding when it is less or near 0.1 and ionic bonding when it is about 0.2. K_2ZnH_4 Rb_2ZnH_4 shows dominantly ionic bonding with a poisson's ratio of 0.1, while Cs_2ZnH_4 has a poison's ratio greater than 0.1 and demonstrates covalent bonding (Surucu et al. 2023). Another parameter Young's modulus, defined the ratio of tensile stress to tensile strain. It represents the stiffness of the materials. Young modulus is the resistance of a material against any change toward x-direction. The stiffness of the materials increases with an increase in the Young modulus (Santhosh and

Table 3 The estimated values of elastic constants (GPa) of K2ZnH4, Rb2ZnH4, and Cs2ZnH4

Materials	C_{11}	C_{22}	C_{33}	C_{44}	C_{55}	C_{66}	C_{12}	C_{13}	C_{23}
K_2ZnH_4	7.27	7.78	11.81	4.78	5.29	3.78	3.78	3.08	2.40
Rb_2ZnH_4	17.25	23.44	20.82	10.89	5.88	5.88	5.88	5.88	5.88
Cs_2ZnH_4	1.85	6.77	2.11	3.20	−0.85	2.98	−2.55	−7.41	−7.28

Table 4 The calculated Bulk modulus B(GPa), Shear modulus G (GPa), Young's modulus E(GPa), Pugh's ratio (B/G) of K_2ZnH_4, Rb_2ZnH_4 and Cs_2ZnH_4

Materials	B	G	E	B/G	υ
K_2ZnH_4	4.22	4.01	9.13	1.05	0.13
Rb_2ZnH_4	16.28	30.85	56.72	0.52	-0.08

Rajeswarapalanichamy 2016). It can be analysed that Rb_2ZnH_4 is much more complex and stiffer than K_2ZnH_4 and Cs_2ZnH_4.

Even though there are compelling scientific and technical arguments for doing so, the mechanical characteristics of the metal hydrides have not been studied in great detail. The design of systems that use hydrides for the storage of hydrogen (such as energy storage, compressors, etc.) must take the response of the hydrides to external stress into consideration because these systems frequently depend on the development of new surfaces for the activation of the hydrides and must deal with the reduction in hydride particle size as the hydrogen is cycled in and out of the system. The hydrogen embrittlement of alloy systems based on hydride-forming metals, such as the group Vb metals (niobium, vanadium, tantalum), is also greatly influenced by the mechanical characteristics of the hydrides (Birnbaum 1984).

3.5 Thermoelectric properties

Thermoelectric properties of the materials are studied to convert thermal energy into electrical energy for practical purposes in detectors and computer cooling systems etc. Heat gradient is produced by the motion of charge as a result of potential difference and creates the thermoelectric effect. Thermoelectric behaviour of the orthorhombic K_2ZnH_4, Rb_2ZnH_4 and Cs_2ZnH_4 (Figs. 6 and 7) has been studied by calculating Seebeck coefficient (S), electrical conductivity (σ), thermal conductivity ($\frac{K_e}{\tau}$), hall coefficient as a function of temperature. The lower values of thermal conductivity and higher values of electrical conductivity and Seebeck coefficient are recommended for better thermoelectric properties.

The thermal conductivity is attributed to the electrons and phonons vibrations in a lattice, and mechanical elastic waves are produced for both due to an increase in temperature. As the electrons being lighter are prone to thermal vibrations in contrast with their phonon vibration, we are considering the thermal conductivity of electrons only. Figure 5a shows the graph of thermal conductivity versus temperature in the range of 0–800 k. The values of thermal conductivity of K_2ZnH_4, Rb_2ZnH_4 and Cs_2ZnH_4 are increasing with the increase of temperature from 0 to 800k. The ($\frac{K_e}{\tau}$) Value of Rb2ZnH4 is greater than the other two compounds due to more considerable energy of electrons (Takeuchi 2009). The heat capacity of compounds versus temperature is shown in Fig. 5b. The heat capacity of solids consists of both phonons and free-charge carriers. Phonons and electrons contribute for indirect band semiconductors while in direct band the contributions only lowered to electrons (Noor et al. 2018a). Heat capacity of the K_2ZnH_4, Rb_2ZnH_4 and Cs_2ZnH_4 incresing with increase of temperature from 0 to 800k. The value of heat capacity is given by Debye law as $C_v \backslash \alpha T^3$, increases linearly with temperature and becomes $C_v = 3R$ at higher temperature, as shown in Fig. 5b.

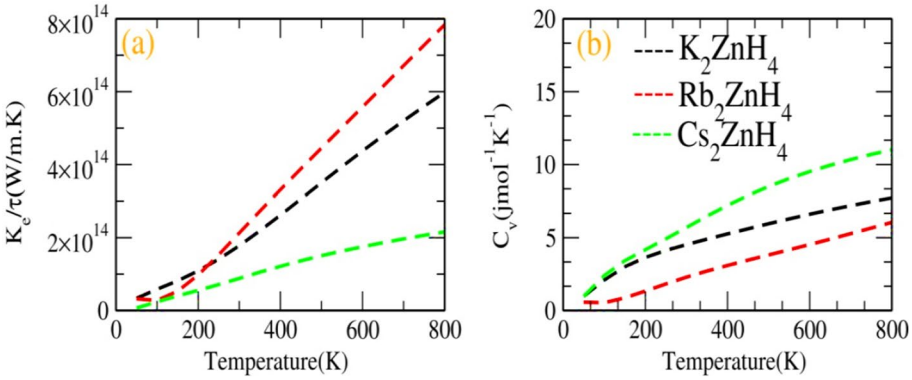

Fig. 6 The calculated (**a**) thermal conductivity, (**b**) specific heat capacity of K_2ZnH_4, Rb_2ZnH_4 and Cs_2ZnH_4 aginst temperature in the range of 0–800 K

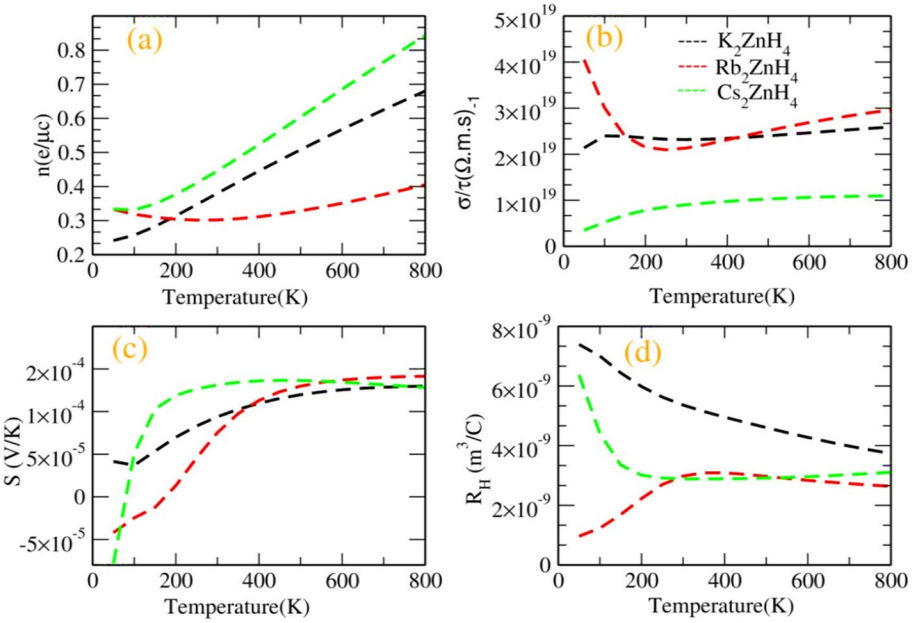

Fig. 7 The calculated values of (**a**) carrier concentration, (**b**) electrical conductivity, (**c**) Seebeck coefficient, (**d**) hall coefficient for K_2ZnH_4, Rb_2ZnH_4 and Cs_2ZnH_4 plotted against temperature in the range of 0–800 K

Thermodynamic study of the compounds K_2ZnH_4, Rb_2ZnH_4 and Cs_2ZnH_4 has been done by exploring the carrier concentration, electrical conductivity, Seebeck coefficient and Hall coefficient aginst temperature in the range of 0–800k as shown in Fig. 6a-d. Figure 6a represents the plot of carrier concentration against temperature which increases with the rise of temperature due to the thermal excitation of electrons. In the case of semiconductors, the fermi level is present between the valence and conduction band and the process of conduction is done by the free carriers due to the electrical conductivity. With the rise

of temperature, more carriers move to the conduction band. In p-type materials, holes and n-type materials, electrons are the majority carriers. The plot of electrical conductivity is increasing linearly above the temperature range from 300 to 800k. The plot of Rb_2ZnH_4 is decreasing from the temperature range of 0-200k due to the metallic behavior of the material below the room temperature (Huma et al. 2021). The Seebeck coefficient defined the ratio of change in voltage as the response of a change in temperature ($S = \frac{\Delta V}{\Delta T}$) (Katz and Poehler 2016). The value of the seebeck coefficient may be positive or negative according to the type of charge; the positive value of the seebeck coefficient represents holes while the negative values of the seebeck coefficient for electrons (Noor et al. 2018b). The Seebeck coefficient of Cs_2ZnH_4 has negative values below the room temperature, which shows the major contribution due to electrons. The estimated values of Seebeck coefficient are shown in Fig. 6c are increasing with temperature increase. The Seebeck coefficient of Cs_2ZnH_4 is greater than K_2ZnH_4 and Rb_2ZnH_4 at room temperature. Lastly, Fig. 6d shows the plot of the hall coefficient against temperature, which demonstrate the effect of free carriers, positive for holes and negative for electrons. The positive values of Hall coefficients agrees well with electronic behavior and Seebeck coefficients, demonstrating p-type nature of the studied materials. Metal hydrides (MH) produce a significant quantity of reaction heat throughout the hydrogen storage and release process. Improving the overall performance of a hydrogen storage unit requires careful consideration of thermal management.

4 Conclusion

The purpose of this study was to search for new zinc hydride crystals with the right combinations of structural, electronic, thermal, and elastic properties for hydrogen storage applications. In the present study, structural, electronic, thermal, and elastic properties of alkali zinc hydrides X_2ZnH_4 ($X = K_2ZnH_4$, Rb_2ZnH_4, and Cs_2ZnH_4) are calculated by the first principle calculations. Structural properties represent that these hydrides are stable in the orthorhombic phase with space group 16- PP222. Electronic band structures and density of states reveal that compounds have electronic semiconducting in order. The nine independent elastic constants for this phase are calculated. Phonon curves shows the thermodynamic stability of materials. Elastic properties are used to investigate the mechanical stability of the materials. The computed elastic constants of K_2ZnH_4 and Rb_2ZnH_4 follow the well-known born stability criteria, suggesting that these materials are mechanically stable while Cs_2ZnH_4 is mechanically unstable. Bulk modulus and shear modulus are used to investigate the resistance of materials towards deformation against volume and shape changes. Both the hydrides show brittle nature, having a poisons ratio lower than 1.75. Mechanical and thermoelectric properties of the studied hydrides are first time investigated and these results are beneficial for further investigation of metal hydrides for the storage of hydrogen in the literature.

Acknowledgements The authors would like to acknowledge the Researchers Supporting Project Number (RSP2024R71), King Saud University Riyadh Saudi Arabia.

Author contributions Conceptualization, Hafeez ur Rehman and Hafiz Hamid Raza; Methodology, Hafeez ur Rehman and Hafiz Hamid Raza; Software, G. Murtaza and Hafeez ur Rehman; Validation, G. Murtaza; Formal Analysis, Nawaz Muhammad; Investigation, Hafeez ur Rehman and Nawaz Muhammad; Resources, G. Murtaza and Nawaz Muhammad; Data Curation, Hafiz Hamid Raza; Writing-Original Draft Preparation, Hafeez ur Rehman; Writing-Review & Editing, Shahid M. Ramay, M. Irfan and M Awais Rehman; Visualization, Nawaz Muhammad and G. Murtaza; Supervision, G. Murtaza and Nawaz Muhammad; Project Administration, G. Murtaza; Funding Acquisition, No.

Funding The authors have not received any funds for this research work.

Declarations

Competing interests The authors declare no competing interests.

Conflict of interest and authorship confirmation form
All authors have participated in (a) conception and design, or analysis and interpretation of the data; (b) drafting the article or revising it critically for important intellectual content; and (c) approval of the final version. This manuscript has not been submitted to, nor is it under review at, another journal or other publishing venue.
The authors have no affiliation with any organisation with a direct or indirect financial interest in the subject matter discussed in the manuscript.

Declaration of interests The authors declare that they have no known competing financial interests or personal relationships that could have appeared to influence the work reported in this paper.

References

Adimi, S., et al.: AB-initio study of pressure-induced aluminum hydrides AAlH4 (A= Li, Na, K, Rb, Cs). Int. J. Hydrog. Energy **42**(40), 25303–25309 (2017)
Al, S., Kurkcu, C., Yamcicier, C.J.: Structural evolution, mechanical, electronic and vibrational properties of high capacity hydrogen storage TiH4. Int. J. Hydrog. Enery **45**(55), 30783–30791 (2020a)
Al, S., Yortanlı, M., Mete, E.: Lithium metal hydrides (Li2CaH4 and Li2SrH4) for hydrogen storage; mechanical, electronic and optical properties. Int. J. Hydrog. Energy **45**(38), 18782–18788 (2020b)
Ali, I.O.A., Joubert, D.P., Suleiman, M.S.J.T.E.P.J.B.: A theoretical investigation of structural, mechanical, electronic and thermoelectric properties of orthorhombic CH 3 NH 3 PbI 3. Eur. Phys. J. B. **91**(10), 1–8 (2018)
Bertheville, B., et al.: Structure data for K2MgH4 and Rb2CaH4 and comparison with hydride and fluoride analogues. J. Alloys Compd. **325**(1–2), L13–L16 (2001)
Birnbaum, H.K.: Mechanical properties of metal hydrides. J. Less Common Met. **104**(1), 31–41 (1984)
Bortz, M., et al.: Synthesis and structure determination of complex zinc hydrides part 1: Dipotassiumtetrahydridozincate (II): K2 [ZnH4]. J. Alloys Compd. **216**(1), 39–42 (1994)
Bortz, M., et al.: Synthesis and structure determination of complex zinc hydrides Part 3. Dirubidium-and dicaesiumtetrahydridozincate (II), Rb2ZnH4 and Cs2ZnH4. J. Alloys Compd. **248**(1–2), L1-L4 (1997)
Broom, D.P.: Hydrogen Storage Materials: The Characterisation of Their Storage Properties. Springer Science & Business Media (2011a)
Broom, D.P.: Hydrogen Storage Materials: The Characterisation of Their Storage Properties, vol. 1. Springer, London (2011b)
Bulusu, A., Walker, D.J.S.: Review of electronic transport models for thermoelectric materials. Superlattices Microstruct. **44**(1), 1–36 (2008)
Chen, X.-F.J.I.: Periodic Density Functional Theory (PDFT) simulating crystal structures with microporous CHA framework: An accuracy and efficiency study. Inorganics **11**(5), 215 (2023)
Chen, X., Yu, T.J.M.: Simulating crystal structure, acidity, proton distribution, and IR spectra of acid zeolite HSAPO-34: A high accuracy study. Molecules **28**(24), 8087 (2023)
Feng, X., et al.: Construction of CdS@ ZnO core–shell nanorod arrays by atomic layer deposition for efficient photoelectrochemical H2 evolution. Sep. Purif. Technol. **324**, 124520 (2023)
Huang, Z., et al.: Constructing one-dimensional mesoporous carbon nanofibers loaded with NaTi2 (PO4) 3 nanodots as novel anodes for sodium energy storage. J. Phys. Chem. Solids **161**, 110479 (2022)
Huang, Z., et al.: Improved electrical resistivity-temperature characteristics of oriented hBN composites for inhibiting temperature-dependence DC surface breakdown. Appl. Phys. Lett. **123**(10) (2023)
Huma, M., et al.: Physical properties of lead-free double perovskites A2SnI6 (A= Cs, Rb) using ab-initio calculations for solar cell applications. Mater. Sci. Semicond. Process. **121**, 105313 (2021)
Hussain, M.I., et al.: Investigations of structural, electronic and optical properties of YInO3 (Y= Rb, Cs, Fr) perovskite oxides using mBJ approximation for optoelectronic applications: A first principles study. Mater. Sci. Semicond. Process. **113**, 105064 (2020)

Jia, L.-C., et al.: Self-standing boron nitride bulks enabled by liquid metals for thermal management. Mater. Horiz. **10**(12), 5656–5665 (2023)
Katz, H.E., Poehler, T.O.: Innovative Thermoelectric Materials: Polymer, Nanostructure and Composite Thermoelectrics. World Scientific (2016)
Kuang, W., et al.: Application of the thermodynamic extremal principle to diffusion-controlled phase transformations in Fe-CX alloys: Modeling and applications. Acta Mater. **159**, 16–30 (2018)
Li, P., et al.: First-principles investigations on structural stability, elastic and electronic properties of Co7M6 (M= W, Mo, Nb) μ phases. Mol. Simul. **45**(9), 752–758 (2019)
Lu, Y., et al.: Mixed-mode operation of hybrid phase-change nanophotonic circuits. Nano Lett. **17**(1), 150–155 (2017)
Lu, C., et al.: BaCo0. 4Fe0. 4Nb0. 1Sc0. 1O3-δ perovskite oxide with super hydration capacity for a high-activity proton ceramic electrolytic cell oxygen electrode. J. Chem. Eng. **472**, 144878 (2023)
Madsen, G.K., Singh, D.J.: BoltzTraP. A code for calculating band-structure dependent quantities. Comput. Phys. Commun. **175**(1), 67–71 (2006)
Murtaza, G., et al.: Lead Free Double Perovsites Halides X2AgTlCl6 (X= Rb, Cs) for solar cells and renewable energy applications. J. Solid State Chem. **297**, 121988 (2021)
Niaz, S., et al.: Hydrogen storage: Materials, methods and perspectives. Renew. Sust. Energ. Rev. **50**, 457–469 (2015)
Noor, N., et al.: Physical properties of cubic BaGeO3 perovskite at various pressure using first-principle calculations for energy renewable devices. J. Mol. Graph. Model. **84**, 152–159 (2018a)
Noor, N., et al.: Investigations of half-metallic ferromagnetism and thermoelectric properties of cubic XCrO3 (X= Ca, Sr, Ba) compounds via first-principles approaches. Phys. Lett. A **382**(42–43), 3095–3102 (2018b)
Pluengphon, P., et al.: Dynamical stabilization and H-vacancy diffusion kinetics of lightweight complex hydrides: Ab initio study for hydrogen storage improvement. Int. J. Hydrog. Energy **46**(43), 22591–22598 (2021)
Pluengphon, P., et al.: Formation of lightweight ternary polyhydrides and their hydrogen storage mechanism. J. Phys. Chem. C **125**(3), 1723–1730 (2021)
Pluengphon, P., et al.: TM dopant-induced H-vacancy diffusion kinetics of sodium-lithium alanates: Ab initio study for hydrogen storage improvement. Int. J. Hydrog. Energy **47**(43), 18763–18771 (2022)
Pugh, S.J.T.L.: XCII. Relations between the elastic moduli and the plastic properties of polycrystalline pure metals. Lond. Edinb. Dublin Philos. Mag. J. Sci. **45**(367), 823–843 (1954)
Qi, X., et al.: Preliminary design of the suppressive containment system based on HPR1000. Nucl. Eng. Des. **415**, 112743 (2023)
Qiu, Y., et al.: Sensitivity improvement in the measurement of minor components by spatial confinement in fiber-optic laser-induced breakdown spectroscopy. Spectrochim. Acta B: at. Spectrosc. **209**, 106800 (2023a)
Qiu, Y., et al.: Plasma dynamics and chlorine emission characteristics on cement pastes using collinear dual-pulse laser-induced breakdown spectroscopy. Spectrochim. Acta B: at. Spectrosc. **209**, 106799 (2023b)
Rehmat, B., et al.: Elastic properties of perovskite-type hydrides LiBeH3 and NaBeH3 for hydrogen storage. Int. J. Hydrog. Energy **42**(15), 10038–10046 (2017)
Reshak, A.H., Jamal, M.: DFT calculation for elastic constants of orthorhombic structure within WIEN2K code: A new package (ortho-elastic). J. Alloys Compd. **543**, 147–151 (2012)
Reshak, A.H., et al.: First-principles calculations of structural, elastic, electronic, and optical properties of perovskite-type KMgH3 crystals: Novel hydrogen storage material. J. Phys. Chem. B **115**(12), 2836–2841 (2011)
Robidas, D., Arivuoli, D.: Reduction of Electron Overflow Problem by Improved InGaN/GaN Based Multiple Quantum Well LEDs Structure with p-AlInGaN/AlGaN EBL Layer. In: Physics of Semiconductor Devices, pp. 189–192. Springer (2014)
Santhosh, M., Rajeswarapalanichamy, R.: Structural phase stability, electronic structure and mechanical properties of alkali metal hydrides AMH4 (A= Li, Na; M= B, AL). J. Phys. Chem. Solids **88**, 68–77 (2016)
Santhosh, M., et al.: First principles study of structural stability, electronic structure and mechanical properties of alkali beryllium hydrides ABeH3 (A= K, Rb, Cs). J. Phys. Chem. Solids **81**, 34–39 (2015)
Sheng, Z., Cheng, M., Wang, J.P.: Multi-wave effects on stability and performance in rotating detonation combustors. Phys. Fluids **35**(7) (2023)
Subhan, F., et al.: Elastic and optoelectronic properties of CaTa2O6 compounds: Cubic and orthorhombic phases. J. Alloys Compd. **785**, 232–239 (2019)
Sukmas, W., et al.: First-principles calculations on superconductivity and H-diffusion kinetics in Mg–B–H phases under pressures. Int. J. Hydrog. Energy **48**(10), 4006–4015 (2023)

Sun, Z., et al.: Enabling low-temperature methanol activation via lattice oxygen induced Cu–O–Cr catalysis. ACS Catal. **13**(20), 13704–13716 (2023)
Surucu, G., et al.: DFT insights into noble gold-based compound Li5AuP2: Effect of pressure on physical properties. ACS Omega **8**(17), 15673–15683 (2023)
Takeuchi, T.: Conditions of electronic structure to obtain large dimensionless figure of merit for developing practical thermoelectric materials. Mater. Trans. 0908170873–0908170873 (2009)
Wang, M., et al.: Reversible calcium alloying enables a practical room-temperature rechargeable calcium-ion battery with a high discharge voltage. Nat. Chem. **10**(6), 667–672 (2018)
Wang, Z., et al.: Improvement of electron transfer efficiency during denitrification process by Fe-Pd/multi-walled carbon nanotubes: Possessed redox characteristics and secreted endogenous electron mediator. Sci. Total. Environ. **781**, 146686 (2021)
Wang, K., et al.: Air plasma-sprayed high-entropy (Y0. 2Yb0. 2Lu0. 2Eu0. 2Er0. 2) 3Al5O12 coating with high thermal protection performance. J. Adv. Ceram. **11**(10), 1571–1582 (2022)
Wang, Y., et al.: Thermal properties of high-entropy RE-disilicates controlled by high throughput composition design and optimization. Mater. Des. **236**, 112485 (2023)
Wimmer, E.: The growing importance of computations in materials science. Current capabilities and perspectives. Mater. Sci. **23**(2), 16 (2005)
Yang, M., et al.: Binocular vision-based method used for determining the static and dynamic parameters of the long-stroke shakers in low-frequency vibration calibration. IEEE Trans. Ind. Electron. **70**(8), 8537–8545 (2022)
Yao, L., et al.: Remarkable synergistic effects of Mg2NiH4 and transition metal carbides (TiC, ZrC, WC) on enhancing the hydrogen storage properties of MgH2. Int. J. Hydrog. Energy **45**(11), 6765–6779 (2020)
Zaluska, A., et al.: Lithium–beryllium hydrides: The lightest reversible metal hydrides. J. Alloys Compd. **307**(1–2), 157–166 (2000)
Zhang, X., et al.: A novel aluminum–graphite dual-ion battery. Adv. Energy Mater. **6**(11), 1502588 (2016)
Zhao, C., Cheung, C.F., Xu, P.: High-efficiency sub-microscale uncertainty measurement method using pattern recognition. IAS Trans. **101**, 503–514 (2020)
Zhao, X.R., et al.: Chloride-promoted photoelectrochemical C—H silylation of heteroarenes. Chin. J. Chem. **41**(22), 2963–2968 (2023)

Authors and Affiliations

Hafeez Ur Rehman[1] · Nawaz Muhammad[1] · G. Murtaza[1] · Hafiz Hamid Raza[1] · Shahid M. Ramay[2] · M. Irfan[3] · M. Awais Rehman[4]

✉ G. Murtaza
gmrai@gcu.edu.pk

✉ Hafiz Hamid Raza
hraza4941@gmail.com

Hafeez Ur Rehman
hafeezurrehmandgk59@gmail.com

Nawaz Muhammad
nawazmuhammad@gcu.edu.pk

Shahid M. Ramay
smramay@yahoo.com

M. Irfan
irfanphy05@gmail.com

M. Awais Rehman
awais12199@gmail.com

[1] Centre for Advanced Studies in Physics, GC University, Lahore, Pakistan

[2] Physics and Astronomy Department, College of Science, King Saud University Riyadh, Riyadh, Saudi Arabia

[3] Departamento de Física Aplicada, Universidade de Vigo, 36310 Vigo, Spain

[4] Institute of Physics, University of Silesia, ul. 75 Pulku Piechoty 1, 41-500 Chorzow, Poland